HHS Public Access

Author manuscript

Ann Diagn Pathol. Author manuscript; available in PMC 2018 October 31.

Published in final edited form as:

Ann Diagn Pathol. 2018 October ; 36: 12–20. doi:10.1016/j.anndiagpath.2018.06.002.

MiR-155 deletion reduces ischemia-induced paralysis in an aortic aneurysm repair mouse model: Utility of immunohistochemistry and histopathology in understanding etiology of spinal cord paralysis

Hamdy Awad[a], **Anna Bratasz**[b], **Gerard Nuovo**[c,*], **Richard Burry**[d], **Xiaomei Meng**[e,1], **Hesham Kelani**[a], **Melissa Brown**[a], **Mohamed E. Ramadan**[a], **Jim Williams**[c], **Lamia Bouhliqah**[f], **Phillip G. Popovich**[d], **Zhen Guan**[d], **Cynthia Mcallister**[g], **Sarah E. Corcoran**[g], **Brian Kaspar**[g], **D. Michele Basso**[h], **José J. Otero**[i], **Claudia Kirsch**[j], **Ian C. Davis**[k], **Carlo Maria Croce**[l], **Jean-Jacques Michaille**[l,m], and **Esmerina Tili**[a,l]

[a]Department of Anesthesiology, Wexner Medical Center, The Ohio State University, Columbus, OH 43210, USA

[b]Small Animal Imaging Center Shared Resource, Wexner Medical Center, OSU, USA

[c]Present address: Phylogeny, Inc., Powell, OH 43065-7295, USA

[d]Department of Neuroscience, The Ohio State University, Columbus, OH 43210, USA

[e]Nationwide Children's Hospital, Columbus, OH 43205, USA

[f]Department of ENT, Wexner Medical Center, OSU, Columbus, OH 43210, USA

[g]Center for Gene Therapy, Nationwide Children's Hospital, Columbus, OH 43205, USA

[h]School of Health and Rehabilitation Sciences, The Ohio State University, Columbus, OH 43210, USA

[i]Department of Pathology, Wexner Medical Center, OSU, Columbus, OH 43210, USA

[j]Department of Radiology, NSUH, 300 Community Drive, Manhasset, NY 11030, USA

[k]Department of Veterinary Biosciences, College of Veterinary Medicine, 1925 Coffey Road, Columbus, OH 43210, USA

[l]Department of Cancer Biology and Genetics, The Ohio State University Wexner Medical Center and Comprehensive Cancer Center, Columbus, OH 43210, USA

[m]BioPerox-IL, UB-INSERM IFR #100, Université de Bourgogne-Franche Comté, Faculté Gabriel, 6 Bd. Gabriel, 21000 Dijon, France

Abstract

[*]Corresponding author. Nuovo.1@osu.edu (G. Nuovo).
[1]Present address.

Potential conflicts of interest
Nothing to report.

Spinal cord paralysis is relatively common after surgical repair of thoraco-abdominal aortic aneurysm (TAAA) and its etiology is unknown. The present study was designed to examine the histopathology of the disease and investigate whether *miR*-155 ablation would reduce spinal cord ischemic damage and delayed hindlimb paralysis induced by aortic cross-clamping (ACC) in our mouse model. The loss of locomotor function in ACC-paralyzed mice correlated with the presence of extensive gray matter damage and central cord edema, with minimal white matter histopathology. qRTPCR and Western blotting showed that the spinal cords of wild-type ACC mice that escaped paralysis showed lower *miR*-155 expression and higher levels of transcripts encoding Mfsd2a, which is implicated in the maintenance of blood-brain barrier integrity. In situ based testing demonstrated that increased miR-155 detection in neurons was highly correlated with the gray matter damage and the loss of one of its targets, Mfsd2a, could serve as a good biomarker of the endothelial cell damage. In vitro, we demonstrated that *miR*-155 targeted Mfsd2a in endothelial cells and motoneurons and increased endothelial cell permeability. Finally, *miR*-155 ablation slowed the progression of central cord edema, and reduced the incidence of paralysis by 40%. In sum, the surgical pathology findings clearly indicated that the epicenter of the ischemic-induced paralysis was the gray matter and that endothelial cell damage correlated to Mfsd2a loss is a good biomarker of the disease. MiR-155 targeting therefore offers new therapeutic opportunity for edema caused by traumatic spinal cord injury and diagnostic pathologists, by using immunohistochemistry, can clarify if this mechanism also is important in other ischemic diseases of the CNS, including stroke.

Keywords

Ischemia; Spinal cord; microRNA; Immunohistochemistry; Histopathology

1. Introduction

During thoraco-abdominal aortic aneurysm (TAAA surgery), the obligatory aortic cross-clamping can lead to inadequate blood supply to the spinal cord, with paraplegia as a possible complication. The rate of paralysis following TAAA repair remains high (5–10%) [1]. The pathophysiology of aortic cross-clamping -induced spinal cord injury, histopathologic changes, and molecular mechanisms leading to paralysis remain largely unknown. Thus, there is no documented bio-marker of the disease that can assist the diagnostic pathologist in a more specific diagnosis. In our mouse model of spinal cord ischemic injury, aortic cross-clamping -induced hindlimb paralysis is a delayed event, with the majority of mice undergoing paralysis approximately 44–48 h following the ischemic event [2]. Therefore, ischemia during surgery does not instantly impair the function of motoneurons. Other events secondary to ischemia either exacerbate the damage on already ischemic motoneurons, or spread the damage to other motoneurons over time. One well characterized secondary event is inflammation, driven in particular by a bimodal release of chemokines whose levels peak at 6 h and then at 36–48 h following reperfusion [3]. Another potential secondary event in our model of delayed paralysis might be endothelial malfunction which could be clarified by the surgical pathology and immunohistochemical profile [4].

Major facilitator superfamily domain containing 2a (Mfsd2a) is implicated in the establishment of a functional blood-brain barrier (BBB) and maintenance of its integrity, and *Mfsd2a*$^{-/-}$ mice present with BBB leakage due to increased transcellular trafficking across endothelial cytoplasm [5]. Of particular interest, Mfsd2a is also the major transporter for the essential omega-3 fatty acid docosahexaenoic acid (DHA) [6] that cannot be synthesized de novo in the brain and must be imported through the BBB to neurons to optimize their function [4].

MicroRNAs are short non-coding RNAs that regulate cellular behavior making them attractive candidates for therapeutic manipulations. The expression of *miR-155* pro-inflammatory microRNA in immune cells is induced by TLR4 and other inflammatory signaling pathways [7]. *TLR4* deletion in mice attenuates the production of pro-inflammatory cytokines and neuronal injury after thoracic aortic occlusion in mice [8]. *MiR-155* has been implicated in vascular diseases, vascular remodeling in acute vascular injury, and angiogenesis [9, 10]. Intravenous injection of a *miR-155* inhibitor reduces brain injury in an experimental mouse stroke model [11]. High levels of *miR-155* are also associated with neuro-inflammatory pathologies such as amyotrophic lateral sclerosis (ALS) and multiple sclerosis (MS), and *miR-155*$^{-/-}$ mice have better prognosis in corresponding models [12–14]. Endothelial cells (ECs) also up-regulate *miR-155* under inflammatory conditions, and *miR-155* has been implicated in BBB dysfunction caused by neuro-inflammation [15]. The in situ detection of miR-155 (and other microRNAs) is well established and can be performed by any diagnostic pathology laboratory [16].

Based on this, we investigated the effects of *miR-155* on spinal cord damage induced by ischemic injury. Using wild-type (WT) and *miR-155* global knockout (*miR-155*$^{-/-}$) mice, we found that *miR-155* activity accelerates the initial development of edema and the spreading of gray matter damage, and increases the rate of paralysis in a mouse model of TAAA patients. These deleterious effects of *miR-155* can at least partially be explained through *miR-155* negative effects on Mfsd2a expression that, thus, provides potential new biomarkers of ischemic damage in the spinal cord to the diagnostic pathologist.

2. Materials and methods

2.1. Animals and patients

The Animal Care and Use Committee at the OSU approved all the experiments with animals. This investigation conforms to the Guide for the Care and Use of Laboratory Animals published by the NIH. Both, C57Bl/6 mice and *miR-155* global knockout (*miR-155*$^{-/-}$) mice in C57Bl/6 background were obtained from Jackson Laboratories. Mice were given standard rodent chow and water ad libitum. Patient study was approved by OSU ethics committee and was conducted in accordance with the Declaration of Helsinki and the patient consented for this study. All analyses conducted on mice were done blindly.

2.2. Aortic cross-clamping

Mice (weight 20–22 g, 10 to 12 weeks old) were anesthetized using 2% isoflurane and placed in the supine position. Surgery was performed on an automatic temperature-adjusting

bed as previously described [2], with body core temperature maintained at 34.5 °C. Two clamps were placed on the descending aorta for 7.5 min. Aortic cross clamping was performed on WT and *miR-155*$^{-/-}$ mice the same day to avoid environmental variations. For surgery, anesthesia was conducted initially with ketamine/xylazine 120/5 mg/kg then maintained with 1.5–2.5% isoflurane in oxygen-enriched air for the duration of the surgical procedure, which usually takes 60–90 min. Rectal temperature was maintained at 34.5 °C using a heated surgical board. Euthanasia procedure meets the guidelines of the 2007 AVMA Guidelines on Euthanasia of Rodent.

2.3. MRI techniques

MRIs were performed at the Small Animal Imaging Center Shared Resource, OSU, using a Bruker Biospec 94/30 scanner operating at a field strength of 9.4 T (Bruker Biospec, Germany). A 4-channels mouse brain receiver-coil and 72 mm volume coil, as a transmitter, was used for high resolution images. The surface coil was placed over dorsal side of mice covering at least T6-L2 spinal cord (SC) level. A 72 mm volume coil was used for longitudinal images. The respiratory rate and rectal temperature were monitored through the experiment with a Small Animal Instrument unit (SAI, Inc., Stonybrook, NY). Results were analyzed blindly.

2.4. Permeability assay

Permeability assay was performed using the In Vitro Vascular Permeability Assay (ECM 642 kit) from Millipore according to the manufacturer's instructions. Briefly, mouse endothelial cells were transfected with either a *pre-miR-Control* or *pre-miR-155*. The day after, endothelial cells were seeded on a collagen-coated insert plate that contains high pore density membrane permitting apical and basolateral access of cells to media. FITC-labeled dextran was added on top of endothelial cells, allowing the fluorescent probe to pass through cell monolayer depending on its permeability. The degree of permeability was determined by measuring the fluorescence of the receiver plate well solution.

2.5. MicroRNA in situ hybridization (ISH)

ISH for *miR-155* was performed by Phylogeny Inc. (Powell, OH), as previously described [16]. Sections were evaluated blindly by the pathologist.

2.6. Immunohistochemistry and co-expression analyses

All sections were dealt with blindly using an automated Leica Bond Max platform. The coverslips of the *miR-155* stained slides were removed and the tissues tested with antibodies of interest for co-expression analyses. The antibodies used for immunohistochemistry were: MFSD2A (#PA5–21049, Invitrogen); ChAT (#AB144P, Millipore); Neuron-Specific Enolase (BML-NA1501–0100, Enzo Life Sciences); CD31 (ab28364, Abcam), and pyruvate dehydrogenase (ab92696, ABCAM).

Co-expression analyses were done using the Nuance system (CRI) as previously published [16]. In brief, a given tissue was tested for two different targets using fast red, NBT/BCIP or DAB as the chromogens. The results were then analyzed by the Nuance and InForm systems

with a with the Zeiss Axioskop microscope to determine what percentage of cells were expressing the two targets of interest.

2.7. Cell cultures and transfection

Mouse endothelial cells prepared as in [17], motoneurons (MN-1 cells) [18] and RAW-264.7 macrophages (ATCC#TIB/71) were cultivated in RPMI-1640 medium. Effects of a pro-inflammatory environment was tested by incubating endothelial or MN-1 cells in presence of supernatant of RAW-264.7 cells that had been either challenged 24 h with lipopolysaccharides (LPS) or mock-treated. Pre-miR™ miRNA Precursor *mmu-miR-155* (#PM13058) and Pre-miR™ miRNA *Precursor Negative Control #1* (#AM17110) were from Ambion/Life technologies (Grand Island, NY).

2.8. Luciferase assays

Fragments of mouse (380 nt) and human (369 nt) *Mfsd2a* 3′UTR were cloned into the pGL3 Luciferase Reporter Vector (Promega, Madison, WI). Each *miR-155* site was subsequently mutated (TAGCAT TAAG, starting at nt #1811 in mouse NM_029662.2 sequence, to TAG CAAAAAG, and GAGCTATTAA, starting at nt #2162 in human NM_001136493.2 sequence, to GAGCTAAAAA, respectively) using the Quick-Exchange Mutagenesis kit (Agilent, Santa Clara, CA).

2.9. Preparation of longitudinal sections

After perfusion, spinal cords were fixed in 4% paraformaldehyde, then incubated for 48 h in 10% (w/v) sucrose. Tissues were embedded in OTC prior to be blindly cryostat sectioned at Children's Hospital (Columbus, OH) and processed for H&E. Mouse spinal cords are ~3 cm long requiring a series of 12–18 micrographs which were pasted together. Spinal cords were embedded with the dorsal side away from the cut surface, so that the ventral surface was sectioned first.

2.10. RNA isolation and quantitative real-time PCR (qRT-PCR)

RNAs were extracted using TRIzol (Invitrogen, Carlsbad, CA). The expression of *miR-155* and *miR-155** was assessed using TaqMan® 002571 and 464539_mat assays, respectively, and that of *Mfsd2a, Cd36, Lpl, Nt5e, Occludin* and *Parp3* with Mm01192211_m1, Mm00432403_m1, Mm00434764_m1, Mm00501910_m1, Mm00500912_m1 and Mm01232604_m1 assays, respectively (Life Technologies, Carlsbad, CA). qRT-PCRs were run in triplicates. Values were normalized using *snoRNA135* or *U6* snRNA for microRNAs, and *βActin* for coding genes.

2.11. Western blots and Affymetrix RNA microarrays

Anti-Mfsd2a (#ab105399) and anti-βActin (#ab49900) antibodies were from Abcam (Cambridge, MA).

Affymetrix microarrays were run at the OSU Microarray Facility (3 mice per group). Data are available at GEO database (#GSE74680).

2.12. Statistics

Statistical analysis of Affymetrix microarrays were done using univariate test. qRT-PCR tests and other quantitative analyses are presented as mean + SD and were compared using two-tailed Student *t*-tests. *P* values are given in legends to figures. The proportions of fully paralyzed WT and *miR-155*$^{-/-}$ mice were compared using a two-samples z-test.

3. Results

3.1. MiR-155 expression increases in neurons and endothelial cells of spinal cord of ACC-paralyzed mice

At 48 h following aortic cross-clamping (ACC), microarrays analysis showed elevated levels of transcripts encoding inflammation markers in the caudal region (i.e., below T6) of the spinal cord of ACC-paralyzed (ACC-P) mice as compared with the spinal cord of sham mice. In agreement with previously published results [2, 3], these findings indicate the presence of inflammatory conditions in the spinal cord of ACC mice, thus establishing the relevance of our ACC mouse model (data not shown). We hypothesized that miR-155 might be associated with ACC-induced paralysis, as previously shown in an experimental mouse model of stroke [11].

In situ hybridization for miR-155 showed that this microRNA was selectively increased in the thoracic and lumbar regions that corresponded to the clinical areas of paralysis (Fig. 1A). Importantly, it was primarily the motorneurons in the ventral horns in the spinal cord of ACC-P mice that expressed miR-155 (Fig. 1B). This was confirmed by co-localization experiments with Neuron-Specific Enolase neuronal marker (Fig. 1C). In contrast, miR-155 was not evident in white matter (Fig. 1D). Interestingly, the pattern of miR-155 expression in the lower thoracic portion of the spinal cord (Fig. 1A) correlated well with the cessation of *NeuN* expression (Fig. 1E) and pyruvate dehydrogenase expression (data not shown), suggesting that miR-155 expression in motoneurons may possibly be linked to their death. In addition, endothelial cells in microvessels located within the gray matter but not white matter of ACC-P mice also contained miR-155 (Fig. 1B, black arrows), which was further confirmed using CD31 (Fig. 1C). At 44–48 h following ACC, the thoracic and lumbar regions of ACC-P mice showed more miR-155-positive cells than the homolog regions of sham mice, giving a further indication that this microRNA is implicated in ischemia-induced damage (Fig. 1F). In addition, at 44–48 h following ACC, the caudal part of the spinal cord of ACC-P mice showed up-regulation of *miR-155* as compared with sham and ACC-non paralyzed (ACC-Non-P) mice 24 h post-surgery (Fig. 1G). Accordingly, an additional set of mice showed higher miR-155 levels in rostral (i.e., above T6) and caudal regions of SC of ACC-P mice than in corresponding regions of ACC-Non-P mice, while the expression of miR-155*, a microRNA produced from the same pre-miRNA as miR-155, remained unaffected (Fig. 1H). Altogether, these results strongly suggested that miR-155 expression in neurons and endothelial cells is implicated in paralysis.

3.2. The spinal cord of WT and miR-155$^{-/-}$ ACC-paralyzed mice present a similar pattern of lesions in the ventral gray matter

To acquire a better understanding of damage caused by ACC to the spinal cord, we used in parallel 10–12 weeks old WT and miR-155$^{-/-}$ mice, also on C57Bl/6 background. At 44–48 h following ACC, no obvious histological damage was found in longitudinal spinal cord sections from sham-operated WT and miR-155$^{-/-}$ mice cut at the level of ventral gray matter, as compared with no-surgery mice (Fig. 2A). The spinal cord of WT and *miR-155*$^{-/-}$ ACC-Non-P mice showed an overall preservation of neurons. In contrast, all WT and *miR-155*$^{-/-}$ fully paralyzed mice presented significantly vacuolated gray matter, with overall white matter sparing (Fig. 2A). At 44–48 h following ACC, there was a 100% concordance between behavior assessment (paralysis) and the appearance of extensive gray matter damage in the spinal cord in both WT and *miR-155*$^{-/-}$ ACC mice (Table 1). No evidence of reactive astrogliosis was noted (Fig. 2B and E). We further found that gray matter damage was not continuous, and areas of "skipping", characterized by morphologically intact neurons, admixed with necrotic/ apoptotic morphology were noted. Interestingly, the size of ischemic lesions in miR-155$^{-/-}$ paralyzed mice remained smaller than those in WT paralyzed mice, while the areas of skipping were larger (compare Fig. 2B and C with Fig. 2E and F, see also Fig. 3C) in all studied animals. Nevertheless, the appearance of vacuolated neurons in miR-155$^{-/-}$ mice was similar to that in WT mice (Fig. 2D and G). Altogether, the presence of similar lesions in the gray matter of the spinal cord of WT and miR-155$^{-/-}$ ACC-P mice showed that miR-155 is not involved in the initiation of the lesions however the frequently smaller size of lesions in the spinal cord of *miR-155*$^{-/-}$ ACC-P mice suggested that this microRNA is likely instrumental in increasing the size of gray matter lesions.

3.3. MiR-155 deletion reduces central cord edema

Since miR-155 expression was up-regulated in endothelial cells (Fig. 1C), we then used MRI to determine whether spinal cord damage may be associated with edema in vivo. Spinal cords of both WT and miR-155$^{-/-}$ ACC-P mice showed a greater amount of increased T2 signal throughout the central gray matter with extension superiorly into the thoracic cord to the cervical level, as well as caudally with significant involvement of the lower thoracic (below T6), lumbar cord and conus (Fig. 3A). The subsequent quantitative 3D volumetric measurement of increased T2 signal, compatible with greatly enlarged central cord edema (CCE) in thoracic and upper lumbar regions of ACC-P mice at 44–48 h, was consistent with histological data (Fig. 2A) and indicative of blood-barrier leakage. As no CCE was found in miR-155$^{-/-}$ mice at 24 h following ACC, we rather compared CCE volume in both strains at 30 h and 44–48 h. Remarkably, CCE volume at 30 h was smaller in *miR-155*$^{-/-}$ mice than in WT ACC-Non-P mice, while at 44–48 h there was no significant CCE volume difference between *miR-155*$^{-/-}$ and WT ACC-P mice (Fig. 3A and B). This suggests that miR-155 might accelerate the initial development of edema. On the other hand, while the proportion of spinal cord injury in ACC-non-P mice remained similar regardless of the genotype, miR-155$^{-/-}$ ACC-P mice presented with reduced SC injury as compared with WT ACC-P mice (Fig. 3C). This result, in agreement with those of Fig. 2, indicates that miR-155 is implicated in spreading of spinal cord damage. We further found that miR-155 increases the relative permeability of a monolayer of mouse endothelial cells (Fig. 3D). Finally, MRI

analyses of two patients at our hospital showed sign of CCE. One of them experienced unilateral lower extremity paresis 3–4 days after TAAA surgery, and presented with edema in the gray matter of the lower thoracic spinal cord with extension to the conus medullaris (Fig. 3E). The patterns of gray matter edema in our mice and patients is strikingly similar, further supporting the rationale that our mouse ACC model is highly relevant to the study of molecular mechanisms of spinal cord damage in patients following TAAA surgery.

3.4. MiR-155 targets Mfsd2a transcripts in neurons and endothelial cells

MicroRNAs potentially target hundreds of transcripts [19–21]. At 24 h after ACC, our microarrays analyses suggested reduced *Mfsd2a* levels in spinal cord of WT ACC-Non-P mice as compared with WT sham mice (data not shown). Given that: (i) Mfsd2a is required for the integrity and function of BBB [5]; (ii) Mfsd2a transports DHA to the brain [6];(iii) The anti-inflammatory Neuroprotectin-D1, known to protect brain and retina against cell injury-induced oxidative stress [22], is produced from DHA; (iv) endothelial cells that overexpress Mfsd2a reduce colitis in mice by generating inflammation-resolving lipid mediators [23]; and(v) The 3′-untranslated region of *Mfsd2a* transcripts contains a *miR-155* target site (www.targetscan.org), we hypothesized that targeting of *Mfsd2a* by *miR-155* may impair termination of inflammatory response and consequently increase CCE and ischemic damage to the spinal cord.

We found increased *Mfsd2a* expression in spinal cord of WT ACCNon-P mice as compared with WT ACC-P and sham mice, suggesting that up-regulating *Mfsd2a* in spinal cord might protect WT ACC mice from paralysis (Fig. 4A). As WT ACC-P mice previously showed enhanced miR-155 expression (Fig. 1H) this suggests that variations of *Mfsd2a* expression in WT mice are at least in part *miR-155*-dependent. In contrast, *Mfsd2a* expression in spinal cord of miR-155$^{-/-}$ mice did not change significantly in ACC-Non-P mice while however increasing in rostral spinal cord of ACC-P mice (Fig. 4A). As Mfsd2a is expressed in both endothelial cells and neurons of mouse brain [5, 6], we checked whether it was also expressed in spinal cord motoneurons. Colocalization experiments with Choline acetyltransferase (ChAT) indeed showed similar levels of *Mfsd2a* expression in motoneurons of spinal cord from sham mice of both genotypes (Fig. 4B). We then assessed the effects of ACC on *Mfsd2a* expression. We observed abundant neurons and endothelial cells expressing Mfsd2a in spinal cords of sham WT and miR-155$^{-/-}$ mice (Fig. 4C). While the numbers of *Mfsd2a*-expressing endothelial cells and neurons 44–48 h after ACC remained similar in ACC-Non-P mice of both genotypes, they were sharply reduced in ACC-P mice of both genotypes (Fig. 4C and D).

In addition, we further found that transfecting mouse endothelial cells with a *miR-155* pre-miRNA reduced *Mfsd2a* transcript levels by roughly 50% (Fig. 5A). A similar result was obtained by cultivating these cells in pro-inflammatory conditions (Fig. 5B). Accordingly, miR-155 reduced the intensity of several protein bands (Fig. 5C) that likely represent differentially glycosylated modified forms of Mfsd2a, as shown for human MFSD2A (see Fig. 2a in [24]). Finally, Luciferase assays in mouse endothelial cells expressing mouse or human *Mfsd2a* 3′-UTR containing either a WT or mutated miR-155 target site suggested

that *miR-155* contributes to limit *Mfsd2a* expression in ischemic conditions, at least in part by directly targeting *Mfsd2a* transcripts (Fig. 5D).

3.5. MiR-155 modulates gene expression in neurons and ECs

We found that pro-inflammatory conditions increase miR-155 expression in both mouse endothelial cells and MN-1 cells (motoneurons) (data not shown). We therefore assessed the effects of over-expressing miR-155 in these cells in the absence or presence of inflammatory conditions. In endothelial cells, miR-155 reduced *Occludin* expression under inflammatory conditions. Both LPS and miR-155 in contrast increased expression of *CD36* and *LPL* (data not shown) two genes up-regulated during stroke [25–27]. In MN-1 cells, LPS increased both *Mfsd2a* and *Nt5e* expression. *MiR-155* impaired up-regulation of both these genes, which might be indicative of deleterious effects of this microRNA in neurons. Finally, miR-155 alone, as well as LPS, up-regulated transcripts encoding Parp3, a factor implicated in in-flammation and cell death [28] (data not shown). These results suggest that CCE and spinal cord damage in ACC mice may be due to simultaneous up-regulation of deleterious genes (miR-155 included) and down-regulation of genes with protective effects.

3.6. MiR-155 deletion significantly reduces the rate of ACC-induced paralysis

The above results suggested that miR-155$^{-/-}$ mice, that presented with smaller CCE at 30 h, should be less likely to experience massive edema and motoneuron loss and therefore less prone to ACC-induced paralysis. Indeed, the deletion of miR-155 reduced the incidence of full paralysis ($P = 0.05$) two days following ACC by roughly 40% (Fig. 6A), with only 14/38 (36.8%) of *miR-155*$^{-/-}$ mice compared to 30/51(58.8%) of WT mice suffering paralysis. Furthermore, 7/51 (13.7%) WT mice as opposed to 2/38 (5.3%) of miR-155$^{-/-}$ mice suffered earlier paralysis (24–28 h post ACC). Of note, neither miR-155$^{-/-}$ nor WT mice did experience paralysis later than 48 h following ACC in our model. These results provide a strong evidence that *miR-155* is instrumental in increasing the risk and accelerating the development of ACC-induced paralysis (Fig. 6).

4. Discussion

This paper details the histologic changes associated with a devastating and relatively common complication of aortic aneurysm repair; spinal cord damage. The data shows that the damage is almost exclusively limited to the gray matter of the lower thoracic and upper lumbar regions of the cord and affects mostly neurons and endothelial cells. We present the first evidence of a direct implication of miR-155 in ACC-induced gray matter edema and paralysis, in particular, but not exclusively, through its targeting of *Mfsd2a* in neurons and endothelial cells. Thus, beyond its pro-inflammatory functions, miR-155 also has multicellular deleterious effects in ACC-induced paralysis, in particular in neurons and endothelial cells of the spinal cord. The implication for the surgical pathologist is that increased miR-155 and/or reduced *Mfsd2a* in neurons and endothelial cells can serve as biomarkers of ischemia-induced spinal cord damage.

We found that miR-155 was up-regulated at 48 h following ACC in spinal cords of paralyzed mice. Although miR-155$^{-/-}$ mice experienced less paralysis than WT mice, ACC-P mice of

both genotypes showed similar, yet not equal, degree of CCE and gray matter damage. This result indicates that miR-155 is not involved in the initiation of ischemic gray matter lesions, but is nevertheless instrumental in increasing the degree and spreading of edema-related spinal cord damage, thus increasing the probability of paralysis by roughly 40%. Interestingly, it was previously found that, following thoracic aortic occlusion, *Tlr4*$^{-/-}$ mice present a reduced functional decline as compared with WT mice, and that the lack of Tlr4 activity translated into a lower level of microglia activation and a reduced production of proinflammatory Il-6 and Tnf [8]. These results further support our own findings, given that miR-155 is under the control of the Tlr4 signaling pathway and enhances Tnf production [7, 29].

MRI analyses further showed evidence of increased T2 signal indicative of central cord edema within the spinal cord of ACC mice that sharply expanded in mice that underwent paralysis. This result sheds light into possible mechanisms responsible for delayed paralysis, and might potentially explain why present neuropreventive strategies failed to further reduce the rate of paralysis in TAAA patients [30]. Of note, increased T2 signal is indicative of central cord edema, and a strong prognosticator of paralysis outcome in patients with spinal cord traumatic injury [31, 32], and vasogenic edema is the main cause of ischemic brain swelling and is closely associated with delayed neuronal death in several animal models of stroke [31, 32]. For the last 20 years, spinal cord edema and spinal compartment syndrome in humans has been postulated as a cause of paralysis after ACC in TAAA repair. Due the lack of clinical studies delineating edema after aortic surgery, this hypothesis is still debated. Nevertheless, the fact that we also found radiographic evidence of increased central gray matter T2 signal on 3 Tesla MRI demonstrating spinal cord edema in two TAAA patients provides the first evidence in support of this hypothesis.

Additionally, the fact that miR-155 deletion slowed the initial development of gray matter edema suggests that miR-155 activity may directly impact molecular pathways implicated in edema progression. In agreement with this hypothesis, we found that the number of endothelial cells and neurons still expressing *Mfsd2a*, was significantly reduced in ACC-P mice of both genotypes as compared with ACC-Non-P mice, however remarkably more in WT than in miR-155$^{-/-}$ ACC-P mice. We also found that *miR-155* increases the relative permeability of a monolayer of endothelial cells. We further found that spinal cords of miR-155$^{-/-}$ ACC-P mice presented with more *Mfsd2a*-expressing cells than SC of WT ACC-P mice, suggesting that miR-155 activity decreases Mfsd2a protective effects in ischemic cords. Furthermore, we present evidence that enhanced miR-155 expression and inflammatory environment reduce the levels of endogenous *Mfsd2a* transcripts in mouse endothelial and motor neuron cells. Mfsd2a has been implicated in both the maintenance of BBB integrity and DHA delivery to the brain [5, 6]. Therefore, our results suggest that miR-155 targeting of *Mfsd2a* may participate to inhibit its up-regulation in WT ACC mice, thus contributing to blood-SC barrier disruption, shown to contribute to early motoneuron degeneration in ALS-model mice [33]. Also, given that anti-inflammatory Neuroprotectin-D1, that protects brain and retina against cell injury-induced oxidative stress [22], is produced from DHA in the brain, it is likely that reduced DHA supply should translate into higher, prolonged inflammatory response to ischemia. Specifically, a recent report showed that Mfsd2a promotes endothelial generation of inflammation-resolving lipid mediators and

reduces colitis [23], a pathology tightly linked to intestinal barrier malfunction and high levels of miR-155 [34]. Thus, Mfsd2a allows to mount a proper anti-in-flammatory response in intestinal vasculature, and accordingly MFSD2A is higher in patients with ulcerative colitis undergoing remission [23]. This results are strikingly similar to our own results showing that WT ACC-NP mice have higher Mfsd2a expression in spinal cord compare to sham or paralyzed mice, further substantiating our hypothesis of Mfsd2a being protective and miR-155 being deleterious in ischemic spinal cords.

Further research will allow us to explore the effects of miR-155 targeting transcripts encoding other factors needed for the integrity of blood-SC barrier, especially proteins implicated in the structure of EC tight junctions. Of note, we found that *miR-155* reduces the expression of occludin in endothelial cells, and it was shown that miR-155 inhibition stabilizes tight junction protein ZO-1, leading to decreased neuronal damage in an experimental mouse stroke model [11]. Of note, the expression of ZO-1 and Occludin is lower in endothelial cells of the blood-spinal cord barrier than in the brain-blood barrier, making the former more susceptible to such damage [35, 36].

Finally, our data additionally suggest that pro-inflammatory and exacerbating effects of miR-155 in ACC-induced paralysis might possibly be secondary to its initiating roles in neurons and endothelial cells, contrary to the essential roles played by macrophage-related pro-in-flammatory effects miR-155 displays in chronic pathologies such as ALS and MS. [10–12] This would explain why miR-155 deletion reduced central cord edema, given that $Tlr4^{-/-}$ mice exhibit improved neurological behavior and reduced edema following global cerebral ischemia/reperfusion [8], and why, similarly to the effects of miR-155 deletion in our model, miR-155 inhibition reduced infarct size by 34% in a mouse model of stroke [11].

In conclusion, our results underscore the importance of in situ based testing in combination with histologic examination on both diagnosing the specific cause of spinal cord damage associated with paralysis and in understanding the etiology. Given that: (i) spinal cord damage due to TAAA repair follows a programmed surgical procedure and occurs in a controlled clinical environment, thus providing a window of opportunity for preventive intervention; (ii) MiR-155 functions in the immune response generally have been well conserved between mouse and human [7]; and (iii) MiR-155 was present in the cerebrospinal fluid of a TAAA patient (Awad H. et al., unpublished data), our results strongly support the translational potential of targeting miR-155 for the prevention and treatment of spinal cord injury after TAAA repair.

Acknowledgements

This work was supported by The National Institutes of Health (RO3NS102861 to E.T., H.A. and A.B.); IRG-67–003-50 to E.T.; OSU College of Medicine Office of Research Discovery Funding Program to E.T. and H.A.; P30-NS04758 to Center for Brain and SC Repair, P30CA16058 to Genomics Facility; and P30-MRI Pilot Project proposal/ OSU/CCTS UL1TR001070 to H.A. by National Institute of Neurological Disorders and Stroke.

References

[1]. Awad H, Ramadan ME, El Sayed HF, et al. Spinal cord injury after thoracic endovascular aortic aneurysm repair. Can J Anaesth 2017;64:1218–35. [PubMed: 29019146]

[2]. Awad H, Ankeny DP, Guan Z, et al. A mouse model of ischemic spinal cord injury with delayed paralysis caused by aortic cross-clamping. Anesthesiology 2010;113:880–91. [PubMed: 20808212]

[3]. Smith PD, Puskas F, Meng X, et al. The evolution of chemokine release supports a bimodal mechanism of spinal cord ischemia and reperfusion injury. Circulation 2012;126:S110–7. [PubMed: 22965970]

[4]. Hamilton JA, Brunaldi K. A model for fatty acid transport into the brain. J Mol Neurosci 2007;33:12–7. [PubMed: 17901540]

[5]. Ben-Zvi A, Lacoste B, Kur E, et al. Mfsd2a is critical for the formation and function of the blood-brain barrier. Nature 2014;509:507–11. [PubMed: 24828040]

[6]. Nguyen LN, Ma D, Shui G, et al. Mfsd2a is a transporter for the essential omega-3 fatty acid docosahexaenoic acid. Nature 2014;509:503–6. [PubMed: 24828044]

[7]. Tili E, Michaille JJ, Croce CM. MicroRNAs play a central role in molecular dys-functions linking inflammation with cancer. Immunol Rev 2013;253:167–84. [PubMed: 23550646]

[8]. Bell MT, Puskas F, Agoston VA, et al. Toll-like receptor 4-dependent microglial activation mediates spinal cord ischemia-reperfusion injury. Circulation 2013;128:S152–6. [PubMed: 24030400]

[9]. Urbich C, Kuehbacher A, Dimmeler S. Role of microRNAs in vascular diseases, in-flammation, and angiogenesis. Cardiovasc Res 2008;79:581–8. [PubMed: 18550634]

[10]. McDonald RA, Hata A, MacLean MR, et al. MicroRNA and vascular remodelling in acute vascular injury and pulmonary vascular remodelling. Cardiovasc Res 2012;93:594–604. [PubMed: 22065733]

[11]. Caballero-Garrido E, Pena-Philippides JC, Lordkipanidze T, et al. In vivo inhibition of miR-155 promotes recovery after experimental mouse stroke. J Neurosci 2015;35:12446–64. [PubMed: 26354913]

[12]. Koval ED, Shaner C, Zhang P, et al. Method for widespread microRNA-155 inhibition prolongs survival in ALS-model mice. Hum Mol Genet 2013;22:4127–35. [PubMed: 23740943]

[13]. Moore CS, Rao VT, Durafourt BA, Bedell BJ, Ludwin SK, Bar-Or A, Antel JP. MiR-155 as a multiple sclerosis-relevant regulator of myeloid cell polarization. Ann Neurol 2013;74:709–20. [PubMed: 23818336]

[14]. Butovsky O, Jedrychowski MP, Cialic R, et al. Targeting miR-155 restores abnormal microglia and attenuates disease in SOD1 mice. Ann Neurol 2015;77:75–99. [PubMed: 25381879]

[15]. Lopez-Ramirez MA, Wu D, Pryce G, et al. MicroRNA-155 negatively affects blood-brain barrier function during neuroinflammation. FASEB J 2014;28:2551–65. [PubMed: 24604078]

[16]. Nuovo GJ, Lee EJ, Lawler S, et al. In situ detection of mature microRNAs by labeled extension on ultramer templates. Biotechniques 2009;46:115–26. [PubMed: 19317656]

[17]. Balconi G, Spagnuolo R, Dejana E. Development of endothelial cell lines from embryonic stem cells: a tool for studying genetically manipulated endothelial cells in vitro. Arterioscler Thromb Vasc Biol 2000;20:1443–51. [PubMed: 10845856]

[18]. Salazar-Grueso EF, Kim S, Kim H. Embryonic mouse spinal cord motor neuron hybrid cells. Neuroreport 1991;2:505–8. [PubMed: 1751804]

[19]. Lim LP, Lau NC, Garrett-Engele P, et al. Microarray analysis shows that some microRNAs downregulate large numbers of target mRNAs. Nature 2005;433:769–73. [PubMed: 15685193]

[20]. Filipowicz W, Jaskiewicz L, Kolb FA, et al. Post-transcriptional gene silencing by siRNAs and miRNAs. Curr Opin Struct Biol 2005;15:331–41. [PubMed: 15925505]

[21]. Tsang J, Zhu J, van Oudenaarden A. MicroRNA-mediated feedback and feedforward loops are recurrent network motifs in mammals. Mol Cell 2007;26:753–67. [PubMed: 17560377]

[22]. Asatryan A, Bazan NG. Molecular mechanisms of signaling via the docosanoid neuroprotectin D1 for cellular homeostasis and neuroprotection. J Biol Chem 2017;292:12390–7. [PubMed: 28615451]

[23]. Ungaro F, Tacconi C, Massimino L, et al. MFSD2A promotes endothelial generation of inflammation-resolving lipid mediators and reduces colitis in mice. Gastroenterology 2017;153:1363–1377.e6. [PubMed: 28827082]

[24]. Alakbarzade V, Hameed A, Quek DQ, et al. A partially inactivating mutation in the sodium-dependent lysophosphatidylcholine transporter MFSD2A causes a non-lethal microcephaly syndrome. Nat Genet 2015;47:814–7. [PubMed: 26005865]

[25]. Kim EH, Tolhurst AT, Szeto HH, Cho SH. Targeting CD36-mediated inflammation reduces acute brain injury in transient, but not permanent, ischemic stroke. CNS Neurosci Ther 2015;21:385–91. [PubMed: 25216018]

[26]. Wang X, Sun W, Xu E. The expression and activity of brain lipoprotein lipase is increased after acute cerebral ischemia-reperfusion in rats. Neuropathology 2010;30:131–9. [PubMed: 19780982]

[27]. Kim M, Ham A, Kim JY, et al. The volatile anesthetic isoflurane induces ecto-5′-nucleotidase (CD73) to protect against renal ischemia and reperfusion injury. Kidney Int 2013;84:90–103. [PubMed: 23423261]

[28]. Pascal JM, Ellenberger T. The rise and fall of poly(ADP-ribose): an enzymatic perspective. DNA Repair (Amst) 2015;32:10–6. [PubMed: 25963443]

[29]. Tili E, Michaille JJ, Cimino A, et al. Modulation of miR-155 and miR-125b levels following lipopolysaccharide/TNF-alpha stimulation and their possible roles in regulating the response to endotoxin shock. J Immunol 2007;179:5082–9. [PubMed: 17911593]

[30]. Acher C, Wynn M. Paraplegia after thoracoabdominal aortic surgery: not just assisted circulation, hypothermic arrest, clamp and sew, or TEVAR. Ann Cardiothorac Surg 2012;1:365–72. [PubMed: 23977522]

[31]. Andreoli C, Colaiacomo MC, Rojas Beccaglia M, et al. MRI in the acute phase of spinal cord traumatic lesions: relationship between MRI findings and neurological outcome. Radiol Med 2005;110:636–45. [PubMed: 16437049]

[32]. Bozzo A, Marcoux J, Radhakrishna M, et al. The role of magnetic resonance imaging in the management of acute spinal cord injury. J Neurotrauma 2011;28:1401–11. [PubMed: 20388006]

[33]. Winkler EA, Sengillo JD, Sagare AP, et al. Blood-spinal cord barrier disruption contributes to early motor-neuron degeneration in ALS-model mice. Proc Natl Acad Sci U S A 2014;111:E1035–42. [PubMed: 24591593]

[34]. Tili E, Michaille JJ, Piurowski V, et al. MicroRNAs in intestinal barrier function, inflammatory bowel disease and related cancers-their effects and therapeutic potentials. Curr Opin Pharmacol 2017;37:142–50. [PubMed: 29154194]

[35]. Ge S, Patcher JS. Isolation and culture of microvascular endothelial cells from murine spinal cord. J Neuroimmunol 2006;177:209–14. [PubMed: 16806499]

[36]. Bartanusz V, Jezova D, Alajajian B, Digicaylioglu M. The blood-spinal cord barrier: morphology and clinical implications. Ann Neurol 2011;70:194–206. [PubMed: 21674586]

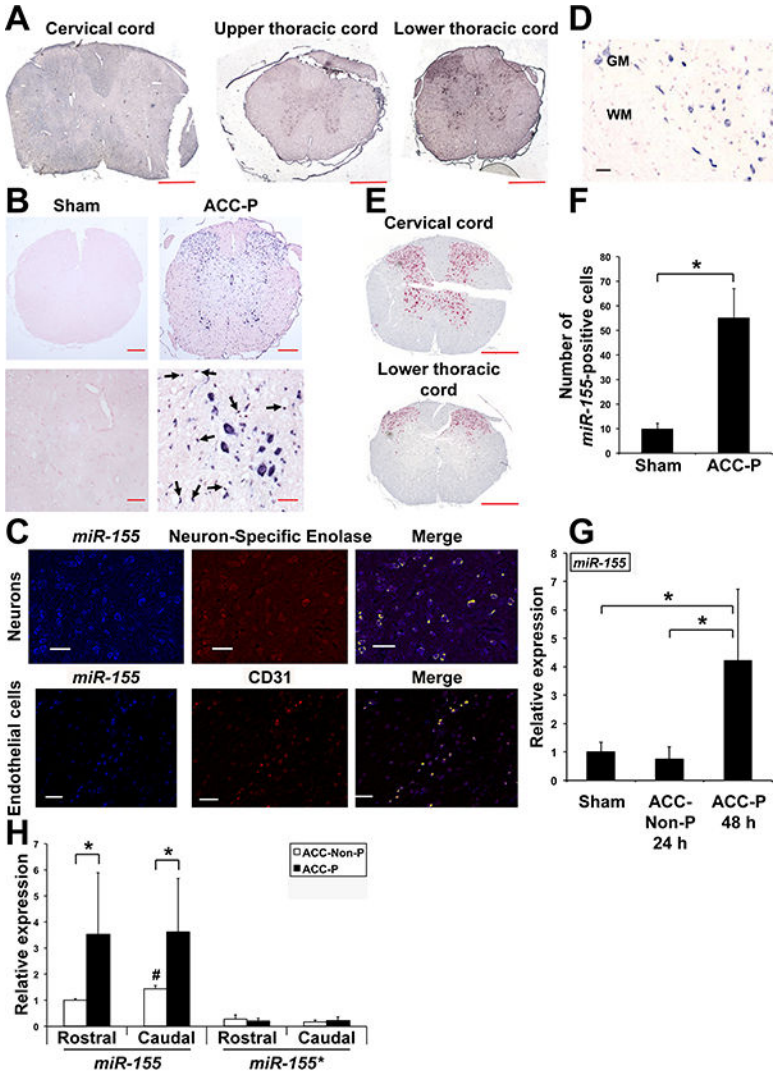

Fig. 1.

Up-regulation of miR-155 expression in SC of ACC-P WT mice. (A) In situ hybridization showing miR-155 expression on three cross sections of spinal cord of the same mouse 48 h following ACC. Scale bars = 400 μm. (B) Representative in situ hybridization for miR-155 on cross sections of the lower thoracic part of SC (44–48 h following ACC) of four sham and four ACC-P mice. Right lower panel: black arrows point to miR-155-positive endothelial cells of blood vessels. Counterstain is nuclear fast red. Top panels: scale bars = 200 μm. Lower panels: scale bars = 40 μm. (C) MiR-155 expression in neurons of WT mice was assessed using an antibody to Neuron-Specific Enolase neuronal marker. *MiR-155* expression in endothelial cells was assessed using an antibody to CD31. Yellow: co-expression. Scale bars = 125 μm. (D) MiR-155 expression in wild type ACC-Paralyzed mice is primarily detected in spinal cord gray matter. WM, White matter. GM, Gray matter. Scale bar = 100 μm. (E) *NeuN* expression in ventral horns of lower thoracic spinal cord following ACC; note loss of expression corresponds to high miR-155 expression. Scale bars = 400 μm. (F) Number (Mean + SD) of miR-155 positive cells on cross-sections of the thoracic and lumbar regions of SC of sham ($n = 4$) and ACC-P ($n = 4$) mice 44–48 h after ACC (3 counts/

mouse). *, $P < 0.0042$. (G) MiR-155 expression (Mean + SD) in the caudal region of the spinal cord of sham ($n = 5$), 24 h ACC-Non-P ($n = 5$) and 44–48 h ACC-P ($n = 4$) WT mice was determined by qRTPCR. *, $P < 0.0459$. Values were normalized to sham. (H) MiR-155 and miR-155* expression (Mean + SD) in the rostral and caudal regions of SC of ACC-Non-P ($n = 4$) and ACC-P ($n = 7$) WT mice was determined by qRT-PCR 44–48 h after ACC. *,$P < 0.031$;#, caudal ACC-Non-P different from rostral ACC-Non-P, $P < 0.0016$. Values were normalized to rostral ACC-Non-P *miR-155*. (For interpretation of the references to colour in this figure legend, the reader is referred to the web version of this article.)

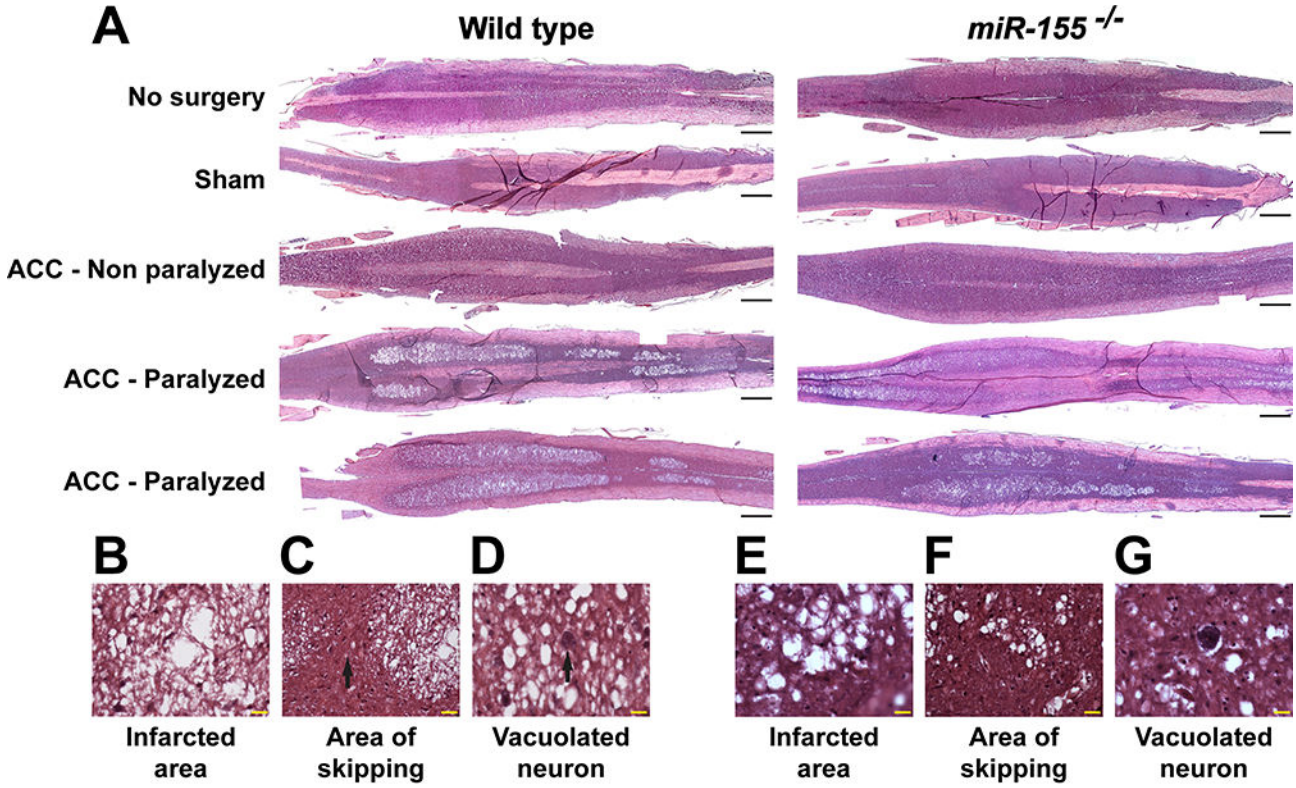

Fig. 2.

Correlation of spinal cord histological damage with paralysis in WT and miR-155$^{-/-}$ ACC mice. (A) Representative images of H&E-stained, longitudinal sections through the ventral horns of spinal cord of no-surgery, sham, ACC-Non-P and ACC-P WT and miR-155$^{-/-}$ mice, 44–48 h following ACC. Rostral is on the right side. Scale bars = 1 mm. (B, E) High definition of the large area of infarct from a WT (B) and a miR-155$^{-/-}$ (E) ACC-P mouse. Scale bars = 20 μm. (C, F) Skipping area [black arrow in (C)] in the same spinal cords as in (B) and (E), respectively, located between two infarcted areas. Scale bars = 20 μm. (D, G) Presence of vacuolated neurons in the same spinal cords as in (B) and (E), respectively. Scale bars = 20 μm.

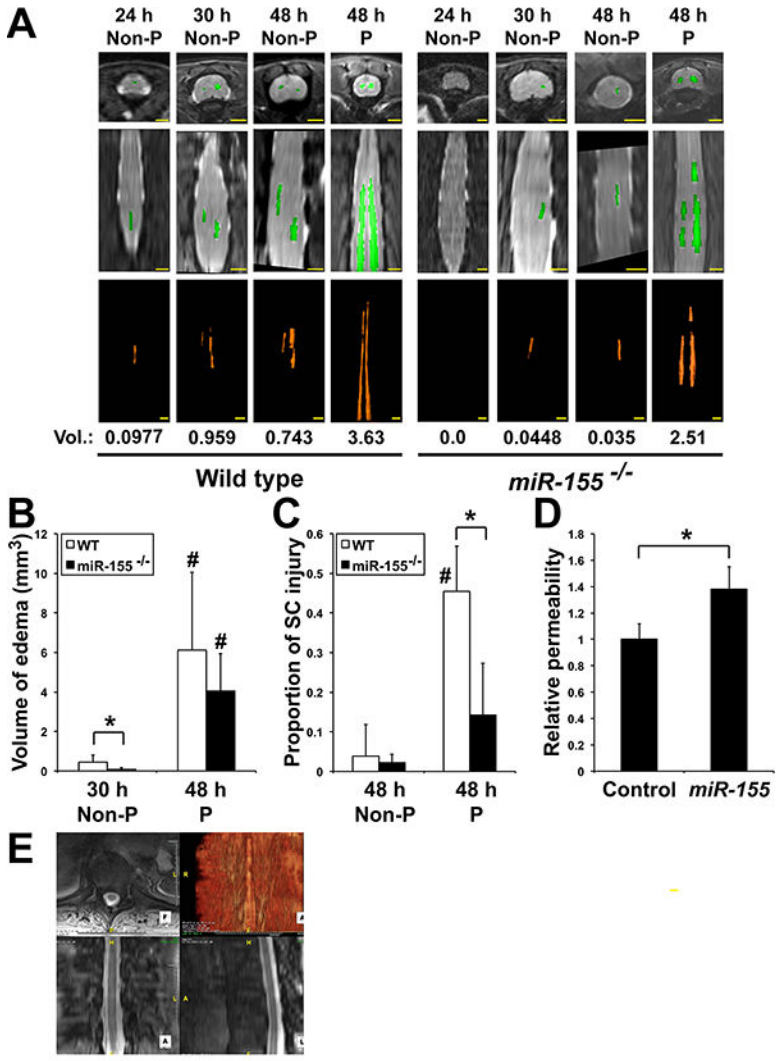

Fig. 3.

MiR-155 interferes with the development of central cord edema (CCE) following ACC. (A) Axial (top panels) and coronal (middle panels) images of T2 weighted WT and miR-155$^{-/-}$ mouse thoracic and lumbar spinal cords as seen by MRI. The volumes (Vol., in mm^3) of increased T2 signal felt to represent CCE (bottom panels) was calculated by outlining areas of increased T2 signal. Scale bars = 2 mm. (B) Volume (Mean + SD) of edema in WT and miR-155$^{-/-}$ ACC mice. *, $P < 0.0455$;$^{\#}$, 48 h paralyzed different from corresponding 30 h Non-P, $P < 0.0049$. At 30 h: WT, $n = 6$; miR-155$^{-/-}$, $n = 8$. At 48 h: WT, $n = 8$; miR-155$^{-/-}$, $n = 6$. (C) Proportion of spinal cord injury (Mean + SD), defined as the ratio of ischemic area/total, in WT (Non-P: $n = 6$; P: $n = 6$) and miR-155$^{-/-}$ (Non-P: $n = 5$; P: $n = 4$) mice 44–48 h after ACC (3 counts/mouse). *, $P < 0.0039$;$^{\#}$, WT paralyzed different from WT non-paralyzed, $P < 0.000046$. (D) Relative permeability of a monolayer of mouse endothelial cells to FITC-Dextran 48 h after transfection with either a control pre-miRNA (Control) or premiR-155 (miR-155). *, $P < 0.0000036$ ($n = 11$ in both groups). Values were normalized to Control. (E) Spinal cord edema in a TAAA repair patient experiencing uni-lateral lower extremity paresis 3–4 days following TAAA repair surgery was analyzed using a Three Tesla

MRI of the thoracic spine utilizing a Siemens Verio scanner with a TR (time to repetition pulse) of 872 ms and TE (time to echo) of 7.8 ms. Three Tesla MRI findings of faint increased T2 signal within central gray matter of the lower thoracic SC extending from T10 to T12 into the conus medullaris and cauda equina, consistent with CCE (volume = 2.96 cm^3). Scale bar = 5 mm (top right panel). Scale bars = 2 mm (three other panels).

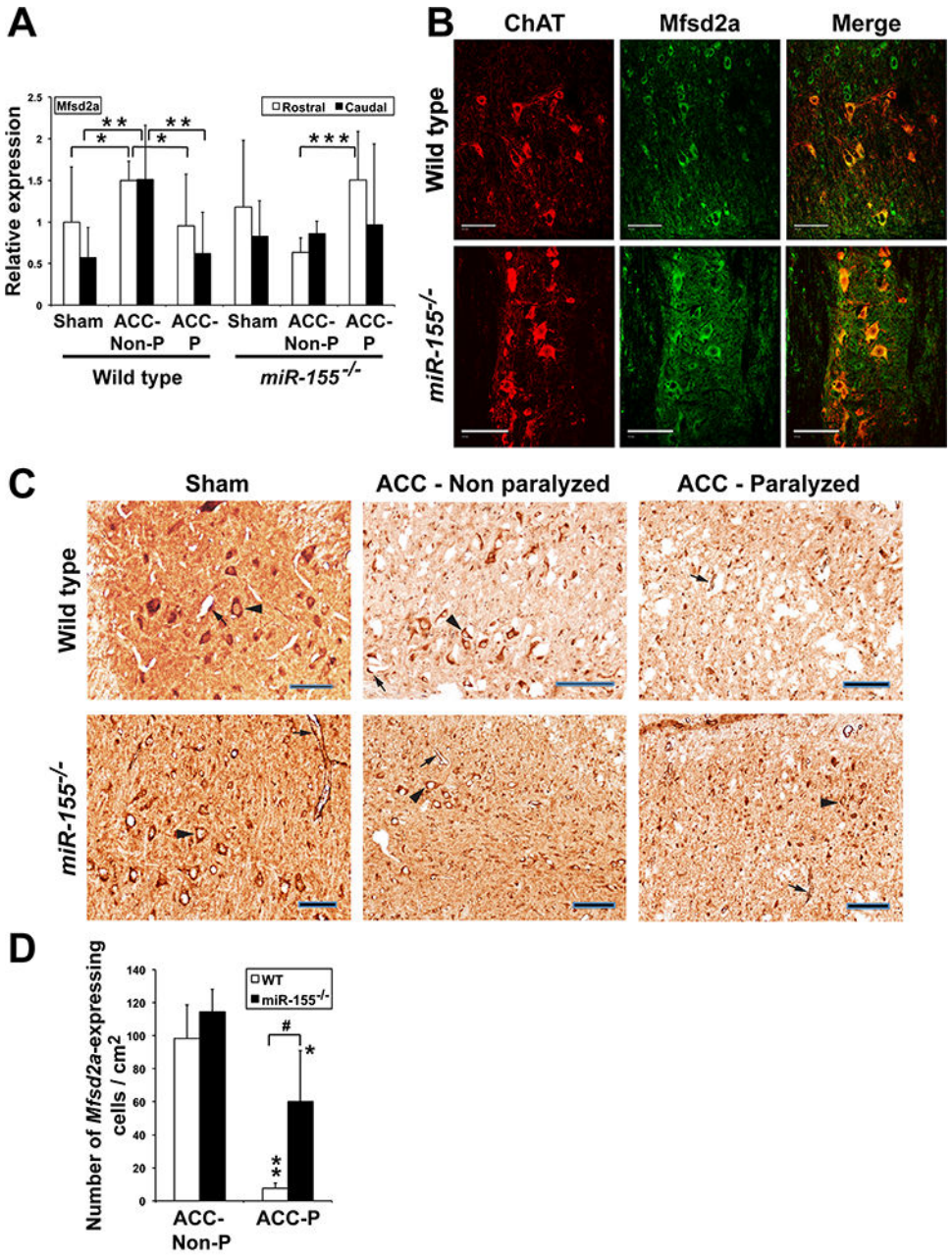

Fig. 4.

Mfsd2a expression is affected by ischemic conditions. (A) *Mfsd2a* relative expression (Mean + SD) 44–48 h after ACC in the rostral and caudal parts of spinal cord of WT sham ($n = 9$), ACC-Non-P ($n = 5$) and ACC-P ($n = 7$) mice, as well as of miR-155$^{-/-}$ sham ($n = 5$), ACC-Non-P ($n = 5$) and ACC-P ($n = 10$) mice, as shown by qRTPCR. *, $P < 0.0668$; **, $P < 0.0361$; ***, $P < 0.00096$. Values were normalized to WT rostral sham. (B) Mfsd2a (green) and ChAT (red), a marker of spinal cord moto-neurons, co-localize (yellow), in both sham WT and sham miR-155$^{-/-}$ mice, as shown by immunohistochemistry. Scale bars = 100 μm. (C) *Mfsd2a*-expressing cells in spinal cord of WT and miR-155$^{-/-}$ mice. Arrow heads: motoneurons. Arrows: endothelial cells. Scale bars = 100 μm. (D) Number of *Mfsd2a*-

expressing endothelial cells and neurons (Mean + SD) 44–48 h after ACC in spinal cord of the same WT and miR-155$^{-/-}$ mice as in Fig. 3C (3 counts/ mouse). ** and *, ACC-P different from corresponding ACC-Non P; **, $P < 0.000093$; *, $P < 0.0312$;$^{\#}$,$P < 0.0027$. (For interpretation of the references to colour in this figure legend, the reader is referred to the web version of this article.)

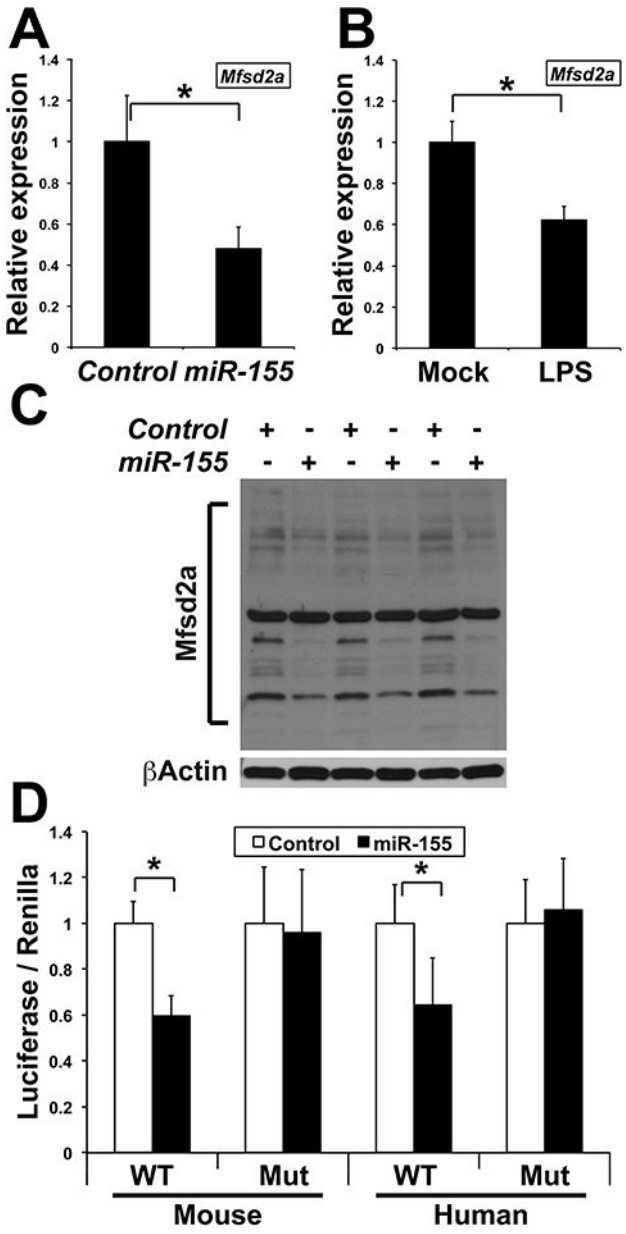

Fig. 5.

MiR-155 targets transcripts encoding Mfsd2a. (A) *Mfsd2a* relative expression (Mean + SD), as determined by qRT-PCR, in mouse endothelial cells transfected with either a control pre-miRNA (*Control*) or pre-miR-155 (miR-155). *, $P < 0.00136$ ($n = 6$ in both groups). Values were normalized to Control. (B) *Mfsd2a* relative expression (Mean + SD), as determined by qRTPCR, in mouse endothelial cells either mock-treated (Mock) or cultivated in the presence of the supernatant of RAW264.7 macrophages challenged with LPS for 24 h (LPS). *, $P < 0.00005$ ($n = 6$ in both groups). Values were normalized to Mock. (C) Western blots showing the expression of multiple Mfsd2a bands in mouse endothelial cells transfected with either a control pre-miRNA (*Control*) or pre-miR-155 (miR-155). Results are from three independent transfection experiments. The main, constant band is most-probably non-

specific. (D) Luciferase activity (Mean + SD) produced from mouse endothelial cells transfected with a *Luciferase* construct containing the mouse or human *Mfsd2a* 3′UTR with either a wild type (*WT*) or *mutated* (*Mut*) *miR-155 target site, along with either a pre-miR-Control (Control) or pre-miR-155 (miR-155). *, P* < 0.033 (*n* = 4 in each group). Values were normalized to Control.

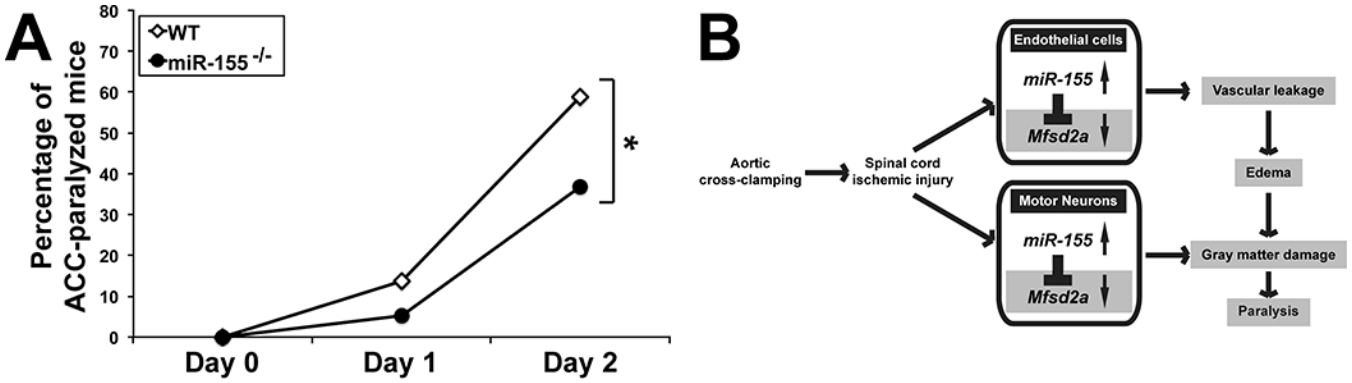

Fig. 6.

(A) MiR-155 deletion reduces the rate of paralysis two days following ACC. Percentages of paralyzed WT ($n = 51$) and miR-155$^{-/-}$ ($n = 38$) mice following ACC. *, $P = 0.05$. (B) Working model showing how miR-155 is instrumental in spreading ischemic damage within the SC. Following ACC, miR-155 targets transcripts encoding *Msfd2a* and other protective factors, which leads to vascular leakage, development of CCE, gray matter damage and paralysis. *Mfsd2a* targeting in neurons is also likely to reduce DHA influx [15], with deleterious consequences on neuron survival and reduced production of anti-inflammatory DHA-derivatives such as Neuroprotectin D1. *MiR-155*$^{-/-}$ ACC-mice retain higher levels of Mfsd2a and other protective factors, thus experiencing slower CCE development, reduced gray matter damage and paralysis. *MiR-155* effects in neurons, particularly on DHA supply under ischemic conditions, remain to be studied.

Table 1

Correlation of behavior with aortic cross-clamping -induced gray matter damage in 10 wild type and 10 *miR-155*$^{-/-}$ mice submitted to histological analysis 44–48 h following the insult.

Genotype	Behavior	Number of mice	Extensive damage
Wild type	Paralyzed	6	6
	Non-paralyzed	4	0
miR-155$^{-/-}$	Paralyzed	3	3
	Non-paralyzed	7	0